https://doi.org/10.5194/egusphere-2026-261
Preprint. Discussion started: 26 May 2026

Non-monotonic response of dust deposition kinetics to low wind speeds

Ruochen Jia[1, 2†], Chaoqun Ba[3†], Chao Zhang[4], Wennong Kuang[5], Yuan Liu[6], Zhigang Wang[6], Fang Liu[6], Zhiming Xin[6], Yuting Liu[6], Qun Ma[1], Lu Zong[7], Wei Liang[1], Jianqiang Qian[8*], Zhimin Liu[1*]

[1] Institute of Applied Ecology, Chinese Academy of Sciences, Shenyang 110016, China.

[2] University of Chinese Academy of Sciences, Beijing 100049, China.

[3] Hebei Minzu Normal University, Chengde 067000, China.

[4] Inner Mongolia University of Finance and Economics, Hohhot, 010070, China.

[5] Beijing Forestry University, Beijing 100083, China.

[6] Experimental Center of Desert Forestry, Chinese Academy of Forestry, Dengkou 015200, China.

[7] Wuhan Botanical Garden, Chinese Academy of Sciences, Wuhan 430074, China.

[8] Henan Agricultural University, Zhengzhou 461101, China.

† These authors contributed equally to this work.

Corresponding author:

Jianqiang Qian

Henan Agricultural University

Zhengzhou, Henan, China, 461101

Email: jq.qian@henau.edu.cn

Phone number: 18604019586

Zhimin Liu

Institute of Applied Ecology, Chinese Academy of Sciences

72 Wenhua Road, Shenyang, Liaoning, China, 110016

Email: zmliu@iae.ac.cn

Phone number: 13840580046

https://doi.org/10.5194/egusphere-2026-261
Preprint. Discussion started: 26 May 2026

Abstract

Dry deposition is a major sink for mineral dust, yet its behavior under weak winds remains poorly constrained and is often parameterized monotonically with wind speed. Here we quantify size-resolved dust deposition kinetics in a large closed-circuit recirculating wind tunnel using a two-stage protocol (brief high-wind loading followed by low-wind deposition at 0, 2, 4, and 6 m s^{-1}). Cumulative deposition time series were measured with an array of collection trays, with the initial suspended dust loading recorded by an online concentration monitor. Particle sizes were characterized by laser diffraction and grouped into six diameter-threshold classes ($PM_{2.5}$–PM_{63}). A first-order kinetic model captured the deposition evolution and yielded an asymptotic cumulative deposition (a), rate coefficient (k), characteristic time scale ($\tau = 1/k$), and initial deposition flux ($J_0 = ak$). Across the tested wind speeds, net deposition for fine-to-medium particles ($PM_{2.5}$–PM_{40}) is highest at 2 m s^{-1} and becomes suppressed at higher speeds, with the strongest evidence for a peaked response in the 30 μm class. Quadratic fits across the four wind-speed levels suggest a potential maximum near 2–3 m s^{-1}. These measurements provide process-based constraints on low-wind dust deposition and highlight a potential intermediate-wind window that can inform and evaluate dry-deposition parameterizations.

Key words: dry deposition; low wind speed; wind tunnel; size-resolved kinetics

1. Introduction

Mineral dust plays a pivotal role in the climate system, terrestrial ecosystems, and human health. It perturbs the atmospheric radiation balance and influences cloud–precipitation processes by scattering and absorbing radiation and acting as cloud condensation nuclei (Kok et al., 2023). Concurrently, it serves as a vital source of long-range nutrient fluxes to both terrestrial and marine ecosystems (Jickells et al., 2005; Mahowald et al., 2010). The atmospheric lifetime and spatial distribution of dust are predominantly governed by dry and wet deposition processes (Tegen & Fung, 2004; Wu et al., 2020). Under large-scale circulation, strong wind episodes produce brief bursts of high dust emission, injecting large amounts of mineral particles into the lower atmosphere over short time scales (Shao, 2008; Kok et al., 2014). As storms subside and near-surface winds transition to a more typical low-speed background state, elevated dust concentrations can persist, making dry deposition the dominant process controlling the final transport distance and atmospheric residence time of particles (Wu et al., 2020; Kok et al., 2021; Mostamandi et al., 2023). Consequently, accurately quantifying deposition efficiency during this post-storm, low-wind phase is crucial for linking source-region emissions to downwind climatic and ecological impacts (Mahowald et al., 2010; Kok et al., 2023).

Over recent decades, most models have simulated dry deposition using a framework that conceptualizes the process as “gravitational settling plus two resistances in series”, in which an aerodynamic resistance and a canopy/surface resistance describe stepwise transfer of particles from the free atmosphere to the underlying surface, allowing for the computation of size-dependent deposition velocities (Slinn, 1982; Wesely et al., 1989; Gallagher et al., 2002; Petroff & Zhang, 2010). Within this framework, particles in the 1–10 μm range are typically considered the least efficiently deposited, associated with the longest transport distances and identified as a critically sensitive size fraction in climate models (Petroff & Zhang, 2010; Zhang & Shao, 2014; Kok et al., 2023). However, a growing body of size-resolved flux observations and model intercomparisons

https://doi.org/10.5194/egusphere-2026-261
Preprint. Discussion started: 26 May 2026

reveals that predicted deposition rates for 0.1–10 μm particles can vary by more than an order of magnitude across dry deposition schemes (Zhang & He, 2014; Bergametti et al., 2018; Emerson et al., 2020), with discrepancies exceeding 200 % even under idealized, homogeneous conditions (Goossens, 2006). These substantial uncertainties propagate directly into estimates of global dust budgets and radiative forcing (Emerson et al., 2020; Kok et al., 2023). Recent systematic evaluations of numerical weather prediction and chemical transport models further demonstrate that differences in dry deposition parameterizations alone can induce systematic biases in simulated dust loads and surface concentrations, even when using identical wind fields and emission sources (Saylor et al., 2019; Zeng et al., 2020; Kong et al., 2025).

Model uncertainties are especially acute under low-wind, weakly turbulent conditions. Both field measurements via eddy-covariance systems and controlled wind-tunnel experiments indicate that for typical background winds (about 2–6 m s^{-1}), dry deposition fluxes do not exhibit a straightforward, monotonic relationship with wind speed. Instead, fluxes appear more sensitive to near-surface turbulence intensity and the particle size distribution (Bergametti et al., 2018; Waza et al., 2019). Furthermore, different samplers and models frequently yield divergent deposition rates at identical wind speeds, and existing schemes often fail to accurately replicate measured deposition fluxes for coarse particles (Petroff & Zhang, 2010; Bergametti et al., 2018; Waza et al., 2019). This evidence challenges the conventional simplification of dry deposition as a process that increases monotonically with wind speed under weak turbulence. It underscores a lack of process-based understanding of the size-selective near-surface transport and deposition of dust under such conditions (Zhang & He, 2014; Emerson et al., 2020).

In contrast to the extensive research on emission and saltation mechanisms during strong winds, the subsequent deposition phase following dust storms has received comparatively less attention. Conventional models often assume that surface dust fluxes decay rapidly to zero once wind speeds fall below the resuspension threshold. This assumption overlooks the potential for complex interactions among aggregation, resuspension, and gravitational settling in weakly turbulent flows (Shao, 2008; Kok et al., 2012). From an aeolian physics perspective, however, a low-wind environment does not signify dynamical quiescence. The post-dust-storm period, characterized by background winds modulated by large-scale circulation and boundary-layer friction, is a common atmospheric state. During this phase, the near-surface turbulent structure remains a key controller of momentum and scalar vertical exchange. Surface properties, such as roughness, soil moisture, and vegetation structure, collectively set the thresholds for dust emission, rebound, and resuspension (Fécan et al., 1999; Shao, 2008; Kok et al., 2012). As wind speed increases from calm conditions, turbulent fluctuations play a dual role: they help maintain particle suspension, delaying settling, while simultaneously enhancing near-surface transport and particle–surface contacts, which can promote both deposition and rebound. At higher wind speeds exceeding the resuspension threshold, saltation and splash processes begin to dominate surface fluxes, potentially inhibit settling or even reversing net deposition (Shao et al., 1993; Shao, 2008; Kok et al., 2012; Zhang & Shao, 2014). This mechanistic reasoning suggests the potential existence of a “low-wind window”, a specific wind speed range where net deposition efficiency reaches a local maximum, outperforming both calm and stronger wind conditions. Current dry deposition parameterizations, however, do not explicitly capture such a non-monotonic response (Petroff & Zhang, 2010; Zhang & He, 2014).

Insights from two-phase flow and hydrodynamics provide further mechanistic support. In suspensions with weak to moderate shear and relatively high particle concentrations, inter-particle

https://doi.org/10.5194/egusphere-2026-261
Preprint. Discussion started: 26 May 2026

collisions and adhesion can induce aggregation, effectively altering the settling size spectrum (Maggi, 2007; Mietta et al., 2009; Zhao et al., 2023; Yu et al., 2022; Penlou et al., 2023). Experiments and numerical simulations consistently show that for fine-particle systems, moderate turbulent shear can significantly enhance bulk settling rates, whereas stronger shear suppresses settling through aggregate breakup and flow dilution (Penlou et al., 2023; Yu et al., 2022). The mean size of particle clusters often exhibits a non-monotonic dependence on shear intensity, peaking at an intermediate level. Recent detailed simulations of cohesive sediment confirm that, within certain parameter ranges, intermediate turbulence intensities can produce the largest flocs, directly illustrating the competition between shear-enhanced aggregation and turbulence-induced breakup (Maggi, 2007; Mietta et al., 2009; Zhao et al., 2023). These findings imply that in the post-storm atmosphere, where near-surface dust concentrations remain high and wind speeds are in low-to-moderate, turbulence may assume a dual function: it maintains particle suspension and enhances horizontal transport, while also facilitating dust–dust collisions and aggregation. This interplay could lead to a peaked, nonlinear relationship between net deposition flux and wind speed (Penlou et al., 2023).

To address this critical knowledge gap, we formulated the hypothesis that dust deposition kinetics under low-wind conditions exhibit a pronounced, size-resolved non-monotonic dependence on wind speed, governed by the competition between two opposing turbulent mechanisms-enhanced particle aggregation and deposition at moderate shear versus suppressed net deposition from incipient resuspension at higher shear. To test this hypothesis, we conducted a series of controlled experiments in a closed-circuit wind tunnel, quantified size-resolved deposition fluxes and the evolution of particle size distributions (PSDs) from an agricultural soil dust under calm air and precisely regulated low-wind speeds (0, 2, 4, and 6 m s^{-1}). An exponential mass-accumulation model was employed to extract key kinetics parameters (e.g. characteristic time constants and deposition rate), which were then systematically correlated with wind speed, particle size, and shifts in PSDs. Our specific objectives were: (1) to determine if an optimal low-wind speed exists for the net deposition of fine and medium particles (e.g., $PM_{2.5}$ – PM_{30}), (2) to identify whether this optimum coincides with observable shifts in PSDs indicative of shear-enhanced aggregation, and (3) to quantify the suppression of fine-particle deposition at higher low-end winds, potentially due to enhanced rebound/resuspension or horizontal export. The findings aim to provide constraints for improving the next generation of dry deposition parameterizations in dust budget and climate models.

2. Materials and Methods

2.1 Wind-tunnel facility and dust preparation

Experiments were conducted in a vertical recirculating wind tunnel at the Desert and Forest Research Station of the Chinese Academy of Forestry in Dengkou, Inner Mongolia, China (Fig. 1a). This closed-loop facility, modified from a conventional open-circuit design, enables continuous circulation of air and suspended dust, thereby facilitating long-duration observations of dust deposition. The test section measures 13 m in length, with a cross section of 2 m (width) × 2 m (height). Flow is driven by four axial fans positioned downstream of the test section, allowing for continuous adjustment of the mean wind speed from 0 to 20 m·s^{-1}. Upstream of the test section, the flow is conditioned by passing through a diffuser, turning vanes, and a settling chamber equipped with honeycombs and screens, collectively ensuring a uniform approach flow with low turbulence

https://doi.org/10.5194/egusphere-2026-261
Preprint. Discussion started: 26 May 2026

intensity and minimal swirl (Xin et al., 2024). The dust used was sourced from the upper 0–5 cm of local cropland soil, which was air-dried and dry-sieved to obtain particles smaller than 63 μm.

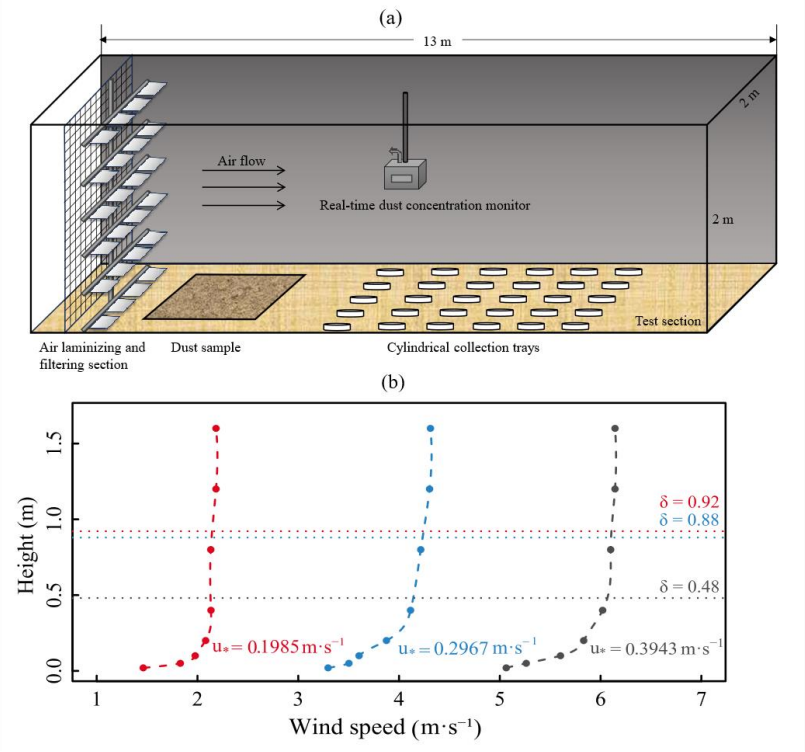

Figure 1. Experimental setup and wind profiles in the closed-circuit wind tunnel.
(a) Schematic layout of the vertical recirculating wind tunnel and sampling section.
(b) Vertical wind-speed profiles measured along the centerline of the test section under nominal approach flows of 2, 4, and 6 m s^{-1}.

2.2 Experimental Procedure

The experimental protocol comprised two sequential stages. (i) Strong-wind loading phase: the wind speed was initially set to 14 m s^{-1} for 5 min to erode the soil source, release dust, and achieve a well-mixed, approximately uniform suspension within the tunnel. (ii) Low-wind deposition phase: the wind speed was then reduced to a target value of 2, 4 or 6 m s^{-1}. Subsequently, 25 cylindrical collection trays (radius: 10 cm, height: 3 cm) were placed on the tunnel floor within the test section. For each wind speed, deposition was sampled at five time intervals (30, 60, 90, 120 and 180 min), with five replicate trays assigned to each interval. Trays were removed at their designated times to obtain the cumulative deposition sample for specific wind-speed–time combination. Additional experiments under quiescent conditions (0 m s^{-1}) were performed in the same test section with fans deactivated, following the same sampling timetable. A real-time dust concentration monitor (Fig. 1a; TD2000A-CT, Zhonggong Tiandi Technology (Beijing) Co., Ltd., Beijing, China) was operated continuously during both the loading and deposition phases to track the bulk suspended dust mass concentration in the test section. The instrument has a measurement range of 0–10 000 mg m^{-3} (RS485 output; DC 24 V). During the 14 m s^{-1} loading phase, the monitor was used as a quality-control indicator of mixing and to ensure that experiments started from comparable initial suspended

https://doi.org/10.5194/egusphere-2026-261
Preprint. Discussion started: 26 May 2026

dust loadings. Immediately after the wind speed was stepped down to the target low-wind value, the monitor reading was recorded as the initial airborne concentration (C_0) for that run, which was used to calibrate the initial-condition comparability across wind-speed treatments and to support subsequent interpretation of the fitted kinetic parameters (Sect. 2.5). For consistency throughout this study, we define particles of 1–10 μm as "fine", 10–20 μm as "medium-sized", and 20–63 μm as "coarse".

2.3 Flow characterization

Vertical wind speed profiles were measured along the tunnel centreline at z = 0.02, 0.05, 0.10, 0.20, 0.40, 0.80, 1.20, and 1.60 m above the floor for nominal approach speeds of 2, 4, and 6 m s^{-1} (Fig. 1b). Friction velocity u_* and aerodynamic roughness length z_0 were obtained by fitting the measured profiles to the logarithmic law of the wall,

$$U(z) = \frac{u_*}{\kappa}\ln\left(\frac{z-d}{z_0}\right),$$

with κ = 0.4. The displacement height d was set to zero for the nominally planar floor, and the fit was restricted to the well-defined surface-layer portion of each profile (excluding the lowest 1–2 measurement points where near-wall effects and probe interference may occur, and excluding points above the boundary-layer thickness). The resulting fits yielded $z_0 \approx 1\times10^{-4}$ m, comparable to values reported for bare sand. The boundary-layer thickness (δ) was estimated using the 99 % of freestream velocity (U_∞) criterion, giving $\delta \approx 0.92$, 0.88, and 0.48 m at 2, 4, and 6 m s^{-1}, respectively (corresponding to δ/z_0 ratios of order 4.8×10^3–9.2×10^3). The top edge of the collection trays was positioned at z = 0.03 m, placing the sampling surface within the surface layer (within 6.3% of δ). No inflection point or abrupt velocity change was detected within 0–5 cm above the trays, indicating minimal flow perturbation by the samplers. While the total tunnel height is 2 m (so that the boundary layer does not fill the entire depth and the upper region is partly influenced by recirculation), the roughness and shear structure within the relevant near-surface layer are reasonably analogous to those of the natural atmospheric surface layer.

2.4 Sample analysis

The mass of deposited dust in each tray was determined using an analytical balance with a resolution of 0.0001 g. Particle-size distributions (PSDs) of the deposited dust were analyzed using a laser diffraction particle-size analyser (Eye Tech, Netherlands). To ensure accuracy and repeatability, the instrument was calibrated before each run using certified reference microspheres (20 μm and 100 nm), requiring agreement between measured and nominal diameters to be within ±1 %. Ultrapure water blanks were analyzed to confirm background noise levels were below 0.5 %. A standard suspension was analysed every 4 h during the measurement; if key parameters like the median diameter (D_{50}) deviated by more than ±2 %, the instrument was recalibrated. All measurements were performed at a circulation speed of 2000 rpm in a temperature-controlled laboratory (23 ± 1 °C). Each tray sample was measured in triplicate, and the average value was used for subsequent analysis.

2.5 Data processing and kinetic modeling

For each wind speed U and time t combination, the total deposited mass per tray was measured and the particle-size distribution (PSD) was recorded. Six size classes ($PM_{2.5}$, PM_{10}, PM_{20}, PM_{30}, PM_{40}, and PM_{63}) are defined by laser-diffraction volume-equivalent diameter thresholds (D_v < 2.5, 10, 20, 30, 40, and 63 μm, respectively); this notation is used for convenience and does not represent

https://doi.org/10.5194/egusphere-2026-261
Preprint. Discussion started: 26 May 2026

aerodynamic PM. The mass of each size class was then calculated as the product of the total deposited mass and its corresponding volume fraction, and converted to an areal cumulative deposition $M(t)$ (mg cm^{-2}) using the known tray area. For each (U, size) combination, five trays were processed; results are summarized by the mean across replicates. The standard error of the mean (SEM, n = 5) at each time point was used as the measurement uncertainty for model fitting.

The temporal evolution of cumulative deposition was represented by a first-order approach to an asymptote,

$$M(t) = a(1 - e^{-kt}),$$

where a (mg cm^{-2}) is the theoretical maximum deposition representing the system's saturated deposition capacity as t→∞. k (h^{-1}) is the deposition-rate coefficient, where larger values indicate a faster approach to saturation. The characteristic deposition time scale was defined as $\tau = 1/k$ (h), corresponding to the time required to reach approximately 63 % a. The initial deposition flux is defined as the initial slope of $M(t)$,

$$J_0 = \left.\frac{dM}{dt}\right|_{t=0} = ak \text{ (mg·cm}^{-2}\text{·h}^{-1}\text{)}.$$

For connection to deposition-velocity formulations used in atmospheric models, dry deposition may be expressed as a downward surface flux $J = V_d C$, where C is the near-surface airborne mass concentration and V_d is the deposition velocity. Under a bulk, vertically well-mixed layer of effective height H_{eff}, $\frac{dC}{dt} = -\left(\frac{V_d}{H_{eff}}\right)C$, implies a first-order form consistent with the expression for $M(t)$. An equivalent deposition velocity was therefore defined by

$$V_{d,eq} = kH_{eff},$$

noting that $V_{d,eq}$ scales linearly with the assumed H_{eff}. In the present facility, a plausible range for H_{eff} spans the measured near-surface boundary-layer thickness ($\delta \approx 0.48-0.92$ m) and the 2 m tunnel height.

Model parameters (a, k) were estimated separately for each wind-speed-size combination by weighted non-linear least squares (NLS), with weights $w_i = 1/SEM_i^2$ applied to the mean at time point t_i. Positive constraints ($a > 0$, $k > 0$) were enforced. Wald 95% confidence intervals for a and k were obtained from the NLS covariance matrix. Uncertainty in the derived metric $J_0 = a \cdot k$ was propagated by the delta method to yield 95% CIs (used in Fig. 3b).

To quantify wind-speed dependence for each size class, J_0 was related to U using linear ($J_0 \sim U$) and quadratic ($J_0 \sim U + U^2$) models; likelihood-ratio tests (LRTs) and ΔAIC were used to evaluate evidence for non-monotonicity. The wind-speed giving the maximum efficiency was summarized by the quadratic vertex $U_{opt} = -\beta_1/(2\beta_2)$, with bootstrap 95% CIs (10,000 resamples of the four (U, J_0) pairs).

Many dry-deposition parameterizations assume that, for a given size and surface type, deposition efficiency (or deposition velocity) increases monotonically with wind speed (or friction velocity), or at most saturates, a strictly non-decreasing reference curve $J_{0,mono}(U)$ was constructed for each size class by isotonic regression fitted to the four (U, J_0) points. Deviations from the monotonic benchmark were summarized by

$$R(U) = \frac{J_0(U)}{J_{0,mono}(U)},$$

where $R > 1$ indicates underprediction by a strictly monotonic scheme and $R < 1$ indicates overprediction at that wind speed.

https://doi.org/10.5194/egusphere-2026-261
Preprint. Discussion started: 26 May 2026

All analyses were performed in R (R Core Team, 2023) (base stats for NLS, boot for resampling, ggplot2 for graphics).

3. Results

3.1 Exponential kinetics of cumulative dust deposition

The first-order exponential model provided an excellent description of the cumulative deposition kinetics for all wind-speed–size combinations, with coefficients of determination (R^2) exceeding 0.91 and approximately 80% of fits achieving R^2 >0.95 (Fig. 2). This confirmed that a single effective time scale adequately characterizes the temporal evolution of dust deposition under experimental conditions.

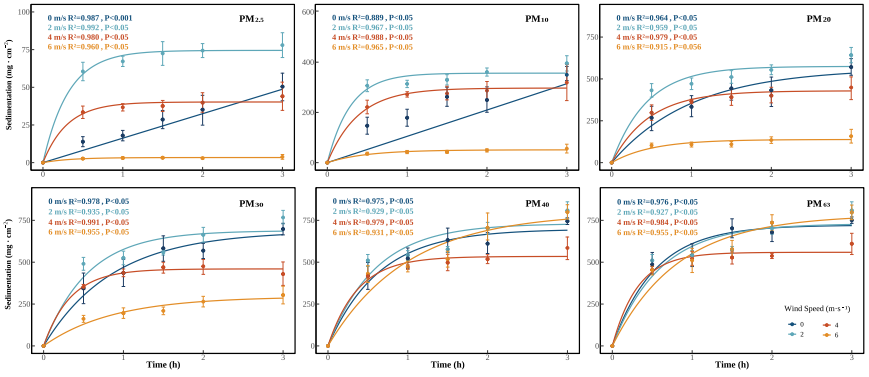

Figure 2. Exponential fits of cumulative deposited mass for different particle-size classes under varying wind speeds.
Each panel corresponds to one dust size class ($PM_{2.5}$–PM_{63}). Symbols represent the mean cumulative deposited mass $M(t)$ (±1 SEM, n = 5 trays) at four wind speeds (0, 2, 4 and 6 m·s^{-1}). Solid curves show non-linear least-squares fits of the first-order exponential model $M(t) = a \cdot (1 - e^{-kt})$. Legends report the coefficient of determination (R^2) and P value for each fit.

Under quiescent conditions (0 m·s^{-1}), fine particles ($PM_{2.5}$, PM_{10}) settled slowly, as evidenced by nearly linear cumulative curves, long characteristic times ($\tau \approx 4.2$ h for $PM_{2.5}$; 1.4 h for PM_{10}), and small rate coefficients (k = 0.24 h^{-1} for $PM_{2.5}$; 0.71 h^{-1} for PM_{10}) (Table S1). In contrast, coarse particles (PM_{30}–PM_{63}) approached saturation within about 1 h (τ < 1 h, $a \approx$ 600–750 mg·cm^{-2}), exhibiting behavior dominated by gravitational settling.

Increasing wind speed from 0 to 2 m·s^{-1} markedly accelerated deposition across all size classes (Tables S1–S2). τ for $PM_{2.5}$ shortened from 4.2 h to 0.3 h (an order-of-magnitude faster approach to saturation), while k increased from 0.24 to 3 h^{-1}. Similarly, for PM_{10}, τ decreased from 1.4 h to 0.3 h and k increased to >3 h^{-1}. For medium and coarse particles, τ also decreased and k increased by factors of roughly 2–4, whereas their asymptotic loads a remained of the same order as under still air (typically within ~20% of the 0 m·s^{-1} values). In contrast, a for $PM_{2.5}$ was reduced by roughly one quarter. These changes indicate that a wind speed of 2 m·s^{-1} strongly enhances deposition kinetics, particularly for fine particles, while maintaining substantial net deposition of medium and coarse particles, representing a low-wind regime that effectively balances deposition rate and total deposited mass.

At 4 m·s^{-1}, τ remained short for all size classes (often < 0.5 h), and k stayed well above still-

https://doi.org/10.5194/egusphere-2026-261
Preprint. Discussion started: 26 May 2026

air values, indicating sustained rapid approach to saturation (Table S1). However, the asymptotic deposition a for all sizes fell below their still-air values, decreasing by roughly 25–60%, especially for fine-to-medium particles. This suppression may reflect increasing competition from particle resuspension and horizontal export at higher shear; because resuspension was not directly measured, we treat this as a plausible interpretation rather than a confirmed mechanism.

At 6 m·s^{-1}, the suppression of net deposition became most pronounced. For $PM_{2.5}$ and PM_{10}, a was reduced by about one order of magnitude relative to still air, indicating near-complete inhibition of effective accumulation despite still-elevated rate coefficients. Deposition of PM_{20} and PM_{30} was also substantially suppressed. In contrast, a for the coarsest fractions (PM_{40}, PM_{63}) was similar to or slightly higher than under still air (within ~10%), but their kinetics were less favorable than at 2–4 m·s^{-1}, with longer τ and lower k compared with the low-wind optimum. Collectively, these results show that high shear maintains large instantaneous settling rates yet strongly suppresses the effective accumulation of fine-to-medium particles, shifting net deposition toward a coarse-dominated regime.

Analysis of characteristic times (Table S1) further shows that for most wind-speed-size combinations, τ is less than 0.5 h, implying that the majority of total deposition occurs within the first 0.5 h. We therefore define 0-0.5 h as the rapid deposition phase and 0.5 – 3 h as the slow deposition phase.

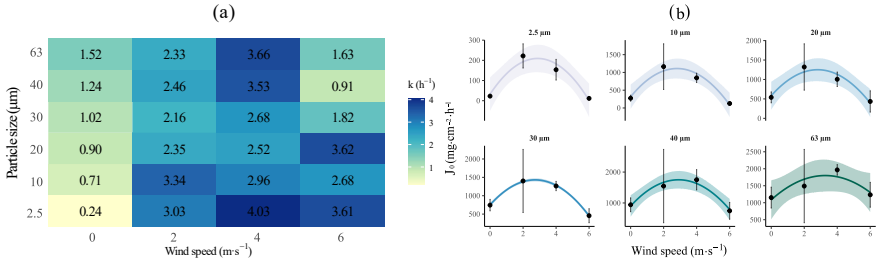

Figure 3. Deposition kinetics and early-stage deposition as functions of wind speed and particle size. (a) Deposition-rate coefficient k (h^{-1}) for each wind-speed-size combination (cell values show k). (b) Initial deposition flux $J_0 = a \cdot k$ versus wind speed U. Points are estimates and error bars are 95% Wald confidence intervals propagated from the weighted NLS fit of $M(t) = a \cdot (1 - e^{-kt})$ with $M(0) = 0, n = 5$ trays per time point). The curve and shaded band show the quadratic fit $J_0 \sim U + U^2$ and its 95% confidence band.

Fig.3 compares deposition dynamics across the parameter space and during the initial stage. Fig.3(a) illustrates the distribution of the rate coefficient k. For fine-to-medium particles ($PM_{2.5}$ – PM_{20}), k reached or approached its maximum at 2 m s^{-1}. At 4–6 m·s^{-1}, k for these sizes decreased slightly. In contrast, the largest k for the coarse fraction (PM_{40}–PM_{63}) occurred at 4 m·s^{-1}. This pattern indicates that weak shear primarily accelerates the deposition of fine-to-medium particles, while moderately higher winds enhance the deposition rate mainly for coarser particles. Fig. 3b shows that J_0 is highest at 2 m s^{-1} among the tested wind speeds for $PM_{2.5}$–PM_{40}, and is strongly reduced at 6 m s^{-1} for the fine size classes. Quadratic fits across the four wind-speed levels yield a model-implied peak wind speed (U_{opt}) around ~2–3 m s^{-1} for several fine-to-medium size classes; bootstrap 95% confidence intervals typically span ~2.3–3.3 m s^{-1} (Table S2). The most pronounced peaked response is found for the 30 μm class, whereas PM_{63} shows weaker evidence for a peak (Table S2).

Synthesizing Fig.3(a) and Fig.3(b), a low-wind window centered near 2 m·s^{-1} (model-inferred optimum around 2–3 m·s^{-1}) simultaneously maximizes the deposition rate (panel a) and the early-stage efficiency (panel b) for $PM_{2.5}$–PM_{30}; stronger winds progressively suppress early deposition

https://doi.org/10.5194/egusphere-2026-261
Preprint. Discussion started: 26 May 2026

of these sizes and shift the net flux toward the coarse fraction.

In summary, dust deposition exhibits a strongly size-selective response to wind speed:

Low wind (2 $m \cdot s^{-1}$, model-inferred optimum between 2–3 $m \cdot s^{-1}$): maximizes the initial deposition flux J_0 and early cumulative deposition for $PM_{2.5}$–PM_{30}.

Moderate wind (4 $m \cdot s^{-1}$): despite relatively high k, both S_0 and early cumulative mass for $PM_{2.5}$–PM_{20} decline compared with 2 $m \cdot s^{-1}$, consistent with enhanced resuspension; coarse particles PM_{40}–PM_{63} approach their rate maximum.

High wind (6 $m \cdot s^{-1}$): markedly suppresses early deposition of $PM_{2.5}$–PM_{20}, and shifts net deposition toward coarse particles, yielding a more coarse-dominated yet overall less efficient early flux.

3.2 Size-selective evolution between rapid and slow deposition stages

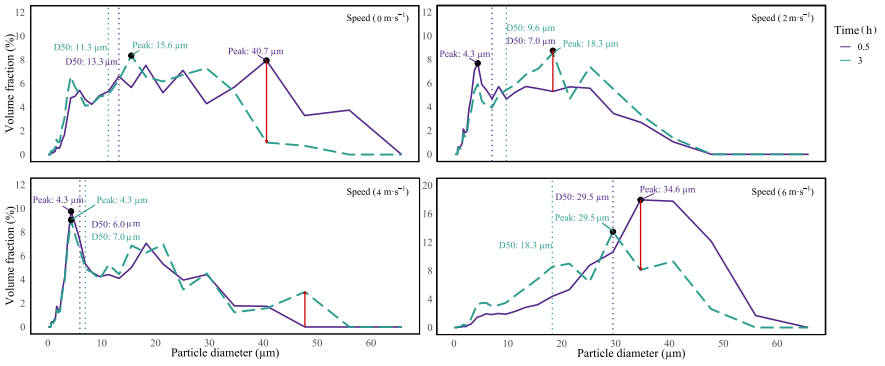

Figure 4. Comparison of deposited particle size distributions (PSDs) between rapid (0–0.5 h) and slow (0.5–3 h) deposition phases under different wind speeds. For each wind speed, the PSD for the two phases are compared. The red vertical line (Δmax) connects the size with the maximal volume fraction difference. "Peak" indicates the modal diameter. Dashed lines mark the median diameter (D_{50}) for each phase.

The particle-size distribution (PSD) of deposited dust evolved distinctly between the rapid (0-0.5 h) and slow (0.5-3 h) deposition phases, reflecting wind-speed-dependent and size selection (Fig. 4).

Under quiescent conditions (0 $m \cdot s^{-1}$), deposited particles at 0.5 h were concentrated around 40 μm (D_{50} = 13.3 μm, peak ≈ 40.7 μm). By 3 h, particles > 30 μm had largely settled, and the PSD contracted into a unimodal distribution dominated by 10–20 μm particles (D_{50} = 11.3 μm, peak ≈ 15.6 μm). This sequence confirms a gravity-dominated regime where coarse particles deposit first, followed by medium-sized particles.

Under low wind (2 m s^{-1}), the median diameter D_{50} increased from 7.0 μm (rapid phase) to 9.6 μm (slow phase), with *a* 37 % increase. This was accompanied by an increased volume fraction at 18 μm (from 6 % to 12 %), indicating a clearer enrichment of medium-sized particles compared to still air. Weak shear thus enhances the deposition of fine particles initially and selectively enriches medium-sized particles later.

Under moderate wind (4 m s^{-1}), the PSDs for the rapid and slow phases were nearly identical, both exhibiting a narrow, persistent peak at 4-5 μm, with D_{50} increasing only slightly from 6.0 to 7.0 μm. This indicates that a fine-particle-dominated size spectrum is established rapidly and

https://doi.org/10.5194/egusphere-2026-261
Preprint. Discussion started: 26 May 2026

remains stable, with subsequent deposition accumulating materials of nearly identical composition.

Under strong wind (6 m s^{-1}), early deposition (0–0.5 h) was dominated by 30–40 μm particles (D_{50} = 29.5 μm, peak ≈ 34.6 μm). By the slow phase (0.5–3 h), the spectrum shifted towards smaller sizes: the primary peak moved to ~29.5 μm, D_{50} decreased to 18.3 μm, a secondary peak emerged in the 10–20 μm range. This demonstrates that under strong shear, coarse particles deposit preferentially early on, with a limited contribution from finer particles later.

In summary, the evolution of deposited PSDs reveals distinct regimes: gravity-controlled sequential settling in still air; shear-enhanced selective enrichment of fine-medium particles at 2 m s^{-1}; rapid establishment of a stable, fine-dominated spectrum at 4 m s^{-1}; and preferential coarse deposition followed by a modest shift to finer sizes at 6 m s^{-1}.

4. Discussion

4.1 Non-monotonic response of dust deposition to low wind speeds

These large-scale closed-circuit wind tunnel experiments suggest a non-monotonic tendency and size-selective response of near-surface dust deposition to low wind speeds (0–6 m s^{-1}). The first-order exponential model $M(t) = a \cdot (1 - e^{-kt})$ captured the cumulative deposition for all size–wind combinations, indicating that net dust deposition can be approximated as a first-order kinetic process governed by a single effective time scale $\tau = 1/k$. The rate coefficient k and its reciprocal τ therefore provide robust dynamical metrics for comparing deposition efficiencies across conditions.

Kinetic parameters show a consistent pattern. Deposition in still air is slow and largely controlled by gravitational settling. The introduction of weak turbulence at 2 m s^{-1} significantly accelerates the deposition of fine-to- medium particles without substantially reducing the maximum deposition of medium-to-coarse particles, creating a distinct low-wind "window" for rapid and efficient dust deposition. Quadratic fits of the initial deposition flux $J_0 = a\ k$ indicate a low-wind optimum at ≈2–3 m s^{-1}, with the strongest response at the experimental level of 2 m s^{-1}. As wind speed increases to 4-6 m s^{-1}, resuspension and horizontal transport may increasingly constrain the mass budget of fine-to-medium particles, strongly suppressing their net deposition and shifting the deposition flux towards a coarse-particle-dominated regime.

Size-resolved PSD evolution further elucidates the size-selective nature of this response. In still air, the deposition spectrum evolves sequentially from coarse to finer particles. Under weak shear (2 m s^{-1}), the median diameter (D_{50}) shifts towards the 10-20 μm range, suggesting that weak turbulence not only accelerates fine-particle deposition but also facilitates their effective "coarsening" during settling, likely through aggregation. In contrast, at higher wind speeds (4-6 m s^{-1}), the deposition spectrum is rapidly stabilized after an initial removal phase, entering a quasi-steady state with minimal total deposition and a gradual spectral shift back toward finer sizes, reflecting the strong suppression of net deposition for fine-to-medium particles.

Synthesizing kinetic parameters and PSD evolution, these lines of evidence show that deposition efficiency is lowest in calm air, optimal around 2 m s^{-1}, and reduced at higher speeds. This low-wind window primarily benefits fine-to-medium particles, whereas for coarse particles it mainly maintains, rather than greatly enhances, their deposition capacity.

4.2 Potential mechanisms underlying the observed deposition patterns

For the respirable fine particles (1–10 μm) central to this study, gravitational settling velocities (ω_s) are only on the order of mm s^{-1}. Their ability to penetrate the thin viscous sublayer adjacent to

https://doi.org/10.5194/egusphere-2026-261
Preprint. Discussion started: 26 May 2026

the surface (thickness $z_v \approx 5\nu/u_* \sim 0.2$–$0.4$ mm) depends critically on the efficiency of turbulent diffusion, expressed by the magnitude of the turbulent diffusive flux $\overline{\omega' c'}$, rather than on gravity alone.

The relative importance of gravitational settling versus turbulent diffusion can be quantified by the Rouse number, $P = \frac{\omega_s}{\kappa u_*}$. For particle diameters of 2-10 μm and the friction velocities (u_*) measured in our study (0.198, 0.297, and 0.394 m s^{-1} at 2, 4, and 6 m s^{-1}, respectively), P falls in the range 10^{-3}–10^{-1} and decreases with increasing wind speed. This confirms that turbulent diffusion becomes increasingly dominant over settling for a given particle size as wind speed increases.

This framework explains the observed optimum: at 2 m s^{-1}, turbulence is sufficient to efficiently transport fine particles from the core flow to the top of the viscous sublayer, maintaining a finite downward flux, yet insufficient to induce substantial resuspension. This creates favorable conditions for deposition. At higher wind speeds (4-6 m s^{-1}), although turbulence transport to the surface remains vigorous, the increased shear stress at the top of the viscous sublayer may promote resuspension and horizontal advection of particles that have reached the near-surface region. This results in high initial deposition rates (large k) but a severely limited ultimate deposition capacity (small a), as observed in this study.

4.2.2 Shear-induced aggregation and effective particle growth

The deposited PSD at 2 m s^{-1} is unique in exhibiting a pronounced shift towards the 10–20 μm range. This "effective coarsening" cannot be explained by turbulent transport alone and points to the role of shear-induced aggregation. The increase in the median diameter (D_{50}) of deposited material from ~7.0 μm (0–0.5 h) to ~9.6 μm (0.5–3 h) corresponds to an effective volume increase by a factor of approximately 2.6, which could be achieved if a fraction of the fine particles deposited as small clusters of only 2–3 primary particles.

This behavior is qualitatively consistent with studies of two-phase turbulent flows and cohesive particles, which often report a non-monotonic relationship between aggregate size and shear intensity, with an optimum intermediate turbulence intensity. Moderate shear can enhance collision frequencies and adhesion, forming transient cluster that increase the ensemble's settling velocity, while stronger shear leads to cluster breakup and reduced net settling (Tian & Ahmadi, 2007; Mietta et al., 2009; Yu et al. 2022; Penlou et al. 2023; Zhao et al. 2023).

While our experimental setup did not allow for direct observation of aggregate morphology, the concurrent evidence-markedly reduced τ, elevated k, and the distinct spectral shift at 2 m s^{-1}-strongly suggests that the enhanced deposition of fine particles is at least partially assisted by shear-related aggregation processes. We therefore posit this as a plausible working hypothesis. Future studies employing microscopic imaging or in-situ cluster statistics are needed to directly quantify this mechanism and its contribution to net deposition.

4.2.3 The possible roles of resuspension

When wind speed increases to 4–6 m s^{-1}, the fitted deposition kinetics exhibit characteristics clearly distinct from those observed at 2 m s^{-1}. For fine particles (1–10 μm), cumulative mass curves over the initial 0.5 h remain relatively steep, and the corresponding rate constants k are not small, indicating that particles are still transported rapidly into the vicinity of the trays and that their contact frequency with the sampling surface is not reduced. However, the asymptotic deposition a decreases

https://doi.org/10.5194/egusphere-2026-261
Preprint. Discussion started: 26 May 2026

markedly with increasing wind speed over time. In contrast, for particles in the 10–20 μm range, a at 6 m s^{-1} is slightly higher than under still air, but the characteristic time scale lengthens substantially; these particles can still complete deposition, but over a longer duration. This pattern is consistent with a regime in which enhanced near-surface shear and turbulence deliver particles to the surface efficiently (large k) while simultaneously increasing the likelihood of rebound and/or removal from the trays, thereby limiting net retained mass (small a). Because upward resuspension fluxes were not directly measured, the relative contributions of resuspension versus horizontal export cannot be separated here and should be tested in future work.

This wind speed feedback on net deposition aligns with previous observations of mineral dust dry deposition and resuspension (Goossens and Rajot, 2008; Bergametti et al., 2018; Waza et al., 2019). Field intercomparison of various passive samplers have demonstrated that dust deposition flux does not always increase monotonically with wind speed; at certain sites and for specific sampler types, apparent net deposition even decreases with increasing wind speed. This inverse relationship is typically attributed to enhanced resuspension fluxes from the surface bed, coupled with increased undercatch of coarse particles by some samplers under high wind conditions (Goossens and Rajot, 2008; Waza et al., 2019). Similarly, wind-tunnel experiments and size-resolved field measurements indicate that near the onset of active wind erosion, particle dry deposition velocities become highly sensitive to friction velocity, surface roughness, and near-surface turbulent structure (Zhang et al., 2014; Bergametti et al., 2018; Waza et al., 2019).

The friction velocities corresponding to 4–6 m s^{-1} in our experiments fall within ranges typically associated with markedly enhanced wind erosion initiation in loess and agricultural soils (Shao, 2008; Sweeney & Mason, 2013). Within this wind-speed interval, increasing near-surface shear stress and turbulence intensity enhance particle delivery to the surface while simultaneously intensifying rebound and resuspension. As a result, a substantial fraction of fine-to-medium particles that have just deposited or are nearing deposition are lifted back into the flow and transported away from the sampling area, leading to a pronounced suppression of net fine-particle deposition efficiency (Goossens & Rajot, 2008; Zhang et al., 2014; Waza et al., 2019).

4.3 Implications for dry-deposition parameterizations and dust budget assessment

Conventional parameterizations of particle dry deposition frequently assume that for a given particle size and surface type, deposition velocity increases monotonically with wind speed or friction velocity, or at most saturates, while resuspension is either treated as an independent flux or represented through simplified empirical coefficients (Zhang et al., 2003; Goossens & Rajot, 2008; Petroff & Zhang, 2010; Kouznetsov & Sofiev, 2012; Zhang & Shao, 2014; Khan & Perlinger, 2017). Although resistance frameworks (Slinn, 1982; Wesely, 1989) provide detailed descriptions of size dependence and surface heterogeneity, they typically do not explicitly account for the “flux peak” and “regime shift” phenomena observed in low-wind, weak-turbulence conditions.

Recent observational and re-parameterization studies (Petroff & Zhang, 2010; Adebiyi & Kok, 2020; Emerson et al., 2020; Farmer et al., 2021) have demonstrated that insufficiently detailed treatment of turbulence intensity and near-surface processes can cause models to overestimate dry-deposition rates of accumulation-mode particles, while underestimating coarse particle deposition, resulting in systematic biases in aerosol lifetime and radiative forcing.

To make the sign and magnitude of the implied bias explicit under a strictly monotonic wind-speed dependence, the observed initial deposition flux J_0 was compared against a non-decreasing

https://doi.org/10.5194/egusphere-2026-261
Preprint. Discussion started: 26 May 2026

benchmark $J_{0,mono}$. The resulting ratios $R(U) = J_0 / J_{0,mono}$ (Table S3) indicate that, for $PM_{2.5}$–PM_{40}, J_0 at $U = 2$ m s^{-1} exceeds the monotonic benchmark by about 15–72% ($R = 1.15 - 1.72$ =), implying that strictly monotonic schemes would underpredict early-stage deposition at low wind speeds. In contrast, at $U = 6$ m s^{-1}, J_0 falls 45–91% below the monotonic benchmark ($R = 0.09 - 0.55$), implying substantial overprediction of net deposition under stronger low-end winds (by factors of ~ 1.8–11 for the affected size classes). Deviations are smaller for PM_{63} ($R \approx 0.77$ at 6 m s^{-1}), suggesting that the non-monotonic response is most pronounced for fine-to-medium particles in the present setup.

This study yields several quantitative insights relevant to dry-deposition parameterizations in the low-wind regime: (i) a distinct peak in the initial deposition flux J_0 occurs at approximately 2 m s^{-1} under a uniform surface conditions, whereas speeds of 4–6 m s^{-1} significantly suppress net deposition of fine–medium particles; (ii) kinetic time scales vary non-monotonically, with the characteristic time τ for fine particles reaching a minimum at 2–4 m s^{-1} while the ultimate maximum deposition a declines sharply at 4–6 m·s^{-1}, indicating that deposition rate and eventual deposited fraction do not vary synchronously with wind speed; (iii) distinct temporal evolution of the PSD emerges, with rapid progression toward the 10–20 μm range at 2 m s^{-1} contrasted against early spectral stabilization at 4–6 m s^{-1}.

These findings complement multi-sampler comparison studies at the Izaña mountain station and evaluations of deposition schemes over rough surfaces (Bergametti et al., 2018; Waza et al., 2019). While previous studies highlighted flux-closure issues from an observation–parameterization discrepancy standpoint, our controlled experiments provide process-level understanding of wind-speed influences. Collectively, these studies demonstrate that representing dry deposition velocity as a monotonic function of wind speed within the 0–6 m s^{-1} range is fundamentally inadequate. Future parameterizations should incorporate size-dependent deposition maxima within weak-turbulence windows and explicitly resolve regime transitions near the resuspension threshold.

From a global dust cycle perspective, this non-monotonicity implies that net dry deposition in source regions under low post-dust wind conditions may be substantially higher than currently modeled, resulting in more rapid atmospheric dust load reduction and shorter effective transport distances. Conversely, under elevated background winds or complex topography, resuspension can extend fine particle residence time and enhance long-range transport fractions. These interpretations align with recent observationally constrained reassessments of dust size distributions and climatic impacts (Kok et al., 2017; Adebiyi & Kok, 2020; Emerson, 2020; Kok et al., 2021, 2023), which consistently identify model tendencies to underestimate coarse dust and near-source deposition while overestimating long-range transport and remote ocean dust burdens. Systematic underestimation of accumulation-mode and coarse particle deposition under weak-to-moderate turbulence would weaken near-source depositional sinks in models, likely resulting in overestimated dust load and radiative effects in remote oceanic and high-latitude regions.

4.4 Uncertainties and future work

Despite controlled experimental conditions with wind speed as the primary variable, several limitations should be acknowledged. First, the use of a single agricultural soil dust (<63 μm), though mineralogically and adhesively representative of specific source regions-limits immediate generalization to dust from other origins such as desert crusts, loess, or urban construction materials, which may exhibit substantially different aggregation potential and resuspension thresholds. Future

https://doi.org/10.5194/egusphere-2026-261
Preprint. Discussion started: 26 May 2026

investigations should incorporate diverse dust types to evaluate the universality of the identified "optimal low-wind deposition" phenomenon.

Second, evidence for shear-induced aggregation remains indirect, derived from deposition kinetics and PSD evolution rather than direct morphological, fractal, or structural characterization of aggregates. Critical parameters including Kolmogorov scales and collision frequencies as functions of wind speed were not explicitly quantified. While observed fine-particle deposition enhancement under weak turbulence is qualitatively consistent with aggregation mechanisms, the quantitative contribution of aggregation to effective settling velocities remains unconstrained. Subsequent research should integrate microscopic imaging, light-scattering spectroscopy, and in situ cluster statistics to characterize deposit structure across wind regimes, enabling direct comparison between experimental cluster-size distributions and two-phase turbulence simulations.

5. Conclusions

This study quantified size-resolved mineral dust dry deposition in a closed-circuit recirculating wind tunnel under calm air and low winds (0–6 m s^{-1}). Across all size–wind combinations, the temporal evolution of cumulative deposited mass is well described by a first-order approach-to-asymptote model ($R^2 > 0.91$), enabling extraction of an asymptotic cumulative deposition (a), deposition-rate coefficient (k), characteristic time scale ($\tau = 1/k$), and initial deposition flux ($J_0 = ak$). These kinetic descriptors provide a compact, process-oriented representation of deposition dynamics that can be compared directly against dry-deposition schemes.

Within the tested wind-speed range, fine-to-medium size classes ($PM_{2.5}$–PM_{40}) show their highest net deposition at 2 m s^{-1} and reduced net deposition at higher winds, with the strongest evidence for a peaked response in the ~30 μm class. The fitted parameters indicate that increasing wind speed can enhance the early-time delivery of particles to the surface (larger k; shorter τ), while the ultimate retained mass on the collection surfaces (a) may decrease under higher low-end winds. Quadratic fits across the four wind-speed levels suggest a potential maximum in net deposition near 2–3 m s^{-1} for several size classes, but the inferred peak location remains tentative given the limited number of wind-speed treatments.

A conceptual interpretation consistent with these patterns is that an intermediate low-wind regime provides sufficient turbulent transport to promote deposition while shear-driven particle rebound, re-entrainment, and horizontal export remain comparatively limited; at higher winds, these competing processes may increasingly constrain the retained deposited mass, effectively decoupling deposition rate from asymptotic loading. Because resuspension fluxes and near-surface particle dynamics were not directly measured in this setup, the relative contributions of rebound/resuspension versus horizontal export cannot be distinguished here and should be evaluated in future experiments with concurrent concentration and flux measurements.

Overall, these measurements offer process-based constraints on dust deposition in the low-wind regime and motivate refinement of dry-deposition parameterizations to represent the possibility of non-monotonic behavior and size-dependent regime shifts. Extending this framework to more realistic boundary-layer turbulence and surface heterogeneity will require targeted observations and simulations that explicitly resolve near-surface transport, retention, and re-entrainment processes.

https://doi.org/10.5194/egusphere-2026-261
Preprint. Discussion started: 26 May 2026

Supplement

The supplement related to this article is available online and includes Tables S1–S3.

Data availability

The data and analysis code supporting this study are archived on Zenodo (https://doi.org/10.5281/zenodo.18264330). The files are under embargo until 30 December 2026, after which they will be made publicly available.

Acknowledgements

This study was supported by the Open Project of Inner Mongolia Academy of Forestry Science (KF2024ZD08), the Natural Science Foundation of Inner Mongolia (2024LHMS03039), the National Natural Science Foundation of China (32401668, 42377458) and the China Postdoctoral Science Foundation (2024M753463). We thank the Experimental Center of Desert Forestry, Chinese Academy of Forestry, for providing the experimental facilities and technical support.

Author contribution

Zhimin Liu, Zhigang Wang, Yuan Liu, and Zhiming Xin conceived the research idea and contributed to the experimental design. Ruochen Jia led the experimental design and execution, performed the data analysis, and wrote the first draft of the manuscript. Chaoqun Ba contributed substantially to the experiments, data processing, and manuscript preparation. Chao Zhang contributed to data analysis and interpretation. Yuting Liu, Qun Ma, Wei Liang and Lu Zong assisted with part of the experimental work. Wennong Kuang and Fang Liu provided critical revisions and constructive comments that improved the manuscript. Jianqiang Qian and Zhimin Liu supervised the study. All authors reviewed and approved the final manuscript.

Competing interests

The authors declare no conflicts of interest.

https://doi.org/10.5194/egusphere-2026-261
Preprint. Discussion started: 26 May 2026

References

[1] Adebiyi, A. A., & Kok, J. F. (2020). Climate models miss most of the coarse dust in the atmosphere. *Science Advances, 6*(15), eaaz9507. https://doi.org/10.1126/sciadv.aaz9507

[2] Bergametti, G., Marticorena, B., Rajot, J.-L., Forêt, G., Alfaro, S. C., & Laurent, B. (2018). Size-resolved dry deposition velocities of dust particles: In situ measurements and parameterizations testing. *Journal of Geophysical Research: Atmospheres, 123*(19). https://doi.org/10.1029/2018JD028964

[3] Donateo, A., & Contini, D. (2014). Correlation of dry deposition velocity and friction velocity over different surfaces for PM2.5 and particle number concentrations. *Advances in Meteorology*, 760393. https://doi.org/10.1155/2014/760393

[4] Emerson, E. W., Hodshire, A. L., DeBolt, H. M., Bilsback, K. R., Pierce, J. R., McMeeking, G. R., & Farmer, D. K. (2020). Revisiting particle dry deposition and its role in radiative effect estimates. *Proceedings of the National Academy of Sciences, 117*(44), 27076–27082. https://doi.org/10.1073/pnas.2014761117

[5] Farmer, D. K., Boedicker, E. K., & DeBolt, H. M. (2021). Dry deposition of atmospheric aerosols: Approaches, observations, and mechanisms. *Annual Review of Physical Chemistry, 72*, 375–397. https://doi.org/10.1146/annurev-physchem-090519-034936

[6] Fécan, F., Marticorena, B., & Bergametti, G. (1999). Parametrization of the increase of the aeolian erosion threshold wind friction velocity due to soil moisture for arid and semi-arid areas. *Annales Geophysicae, 17*(1), 149–157. https://doi.org/10.1007/s00585-999-0149-7

[7] Gallagher, M. W., Nemitz, E., Dorsey, J. R., Fowler, D., Sutton, M. A., Flynn, M., & Duyzer, J. H. (2002). Measurements and parameterizations of small aerosol deposition velocities to grassland, arable crops and forest: Influence of surface roughness length on deposition. *Journal of Geophysical Research: Atmospheres, 107*(D12), AAC 8-1-AAC 8-10. https://doi.org/10.1029/2001JD000817

[8] Goossens, D. (2006). Aeolian deposition of dust over hills: The effect of dust grain size on the deposition pattern. *Earth Surface Processes and Landforms, 31*(6), 762–776. https://doi.org/10.1002/esp.1272

[9] Goossens, D., & Rajot, J. L. (2008). Techniques to measure the dry aeolian deposition of dust in arid and semi-arid landscapes: A comparative study in West Niger. *Earth Surface Processes and Landforms, 33*(2), 178–195. https://doi.org/10.1002/esp.1533

[10] Jickells, T. D., An, Z. S., Andersen, K. K., Baker, A. R., Bergametti, G., Brooks, N., Cao, J. J., Boyd, P. W., Duce, R. A., Hunter, K. A., Kawahata, H., Kubilay, N., LaRoche, J., Liss, P. S., Mahowald, N., Prospero, J. M., Ridgwell, A. J., Tegen, I., & Torres, R. (2005). Global iron connections between desert dust, ocean biogeochemistry, and climate. *Science*, 308(5718), 67–71. https://doi.org/10.1126/science.1105959

[11] Khan, T. R., & Perlinger, J. A. (2017). Evaluation of five dry particle deposition parameterizations for incorporation into atmospheric transport models. *Geoscientific Model Development, 10*, 3861–3888. https://doi.org/10.5194/gmd-10-3861-2017

[12] Kok, J. F., Adebiyi, A. A., Albani, S., Balkanski, Y., Checa-Garcia, R., Chin, M., Colarco, P. R., Hamilton, D. S., Huang, Y., Ito, A., Klose, M., Li, L., Mahowald, N. M., Miller, R. L., Obiso, V., Pérez García-Pando, C., Rocha-Lima, A., & Wan, J. S. (2021). Contribution of the world's main dust source regions to the global cycle of desert dust. *Atmospheric Chemistry and Physics*, 21, 8169–8193. https://doi.org/10.5194/acp-21-8169-2021

https://doi.org/10.5194/egusphere-2026-261
Preprint. Discussion started: 26 May 2026

[13] Kok, J. F., Albani, S., Mahowald, N. M., & Ward, D. S. (2014). An improved dust emission model – Part 2: Evaluation in the Community Earth System Model, with implications for the use of dust source functions. *Atmospheric Chemistry and Physics*, 14, 13043–13061. https://doi.org/10.5194/acp-14-13043-2014

[14] Kok, J. F., Parteli, E. J. R., Michaels, T. I., & Karam, D. B. (2012). The physics of wind-blown sand and dust. *Reports on Progress in Physics, 75*(10), 106901. https://doi.org/10.1088/0034-4885/75/10/106901

[15] Kok, J. F., Ridley, D. A., Zhou, Q., Miller, R. L., Zhao, C., Heald, C. L., Ward, D. S., Albani, S., & Haustein, K. (2017). Smaller desert dust cooling effect estimated from analysis of dust size and abundance. *Nature Geoscience*, 10, 274–278. https://doi.org/10.1038/ngeo2912

[16] Kok, J. F., Storelvmo, T., Karydis, V. A., Adebiyi, A. A., Mahowald, N. M., Evan, A. T., He, C., & Leung, D. M. (2023). Mineral dust aerosol impacts on global climate and climate change. *Nature Reviews Earth & Environment*, *4*, 71–86. https://doi.org/10.1038/s43017-022-00379-5.

[17] Kong, S. S.-K., Fu, J. S., Lin, N.-H., Sheu, G.-R., & Huang, W.-S. (2025). Modeling CMAQ dry deposition treatment over the western Pacific: A distinct characteristic of mineral dust and anthropogenic aerosols. *Atmospheric Chemistry and Physics, 25*, 7245–7268. https://doi.org/10.5194/acp-25-7245-2025

[18] Kouznetsov, R., & Sofiev, M. (2012). A methodology for evaluation of vertical dispersion and dry deposition of atmospheric aerosols. *Journal of Geophysical Research: Atmospheres*, *117*, D01202. https://doi.org/10.1029/2011JD016366

[19] Maggi, F., Mietta, F., & Winterwerp, J. C. (2007). Effect of variable fractal dimension on the floc size distribution of suspended cohesive sediment. *Journal of Hydrology, 343,* 43–55. https://doi.org/10.1016/j.jhydrol.2007.05.035

[20] Mahowald, N. M., Kloster, S., Engelstaedter, S., Moore, J. K., Mukhopadhyay, S., McConnell, J. R., Albani, S., Doney, S. C., Bhattacharya, A., Curran, M. A. J., Flanner, M. G., Hoffman, F. M., Lawrence, D. M., Lindsay, K., Mayewski, P. A., Neff, J., Rothenberg, D., Thomas, E., Thornton, P. E., & Zender, C. S. (2010). Observed 20th century desert dust variability: Impact on climate and biogeochemistry. *Atmospheric Chemistry and Physics, 10*(22), 10875–10893. https://doi.org/10.5194/acp-10-10875-2010

[21] Mietta, F., Chassagne, C., Manning, A. J., & Winterwerp, J. C. (2009). Influence of shear rate, organic matter content, pH and salinity on mud flocculation. *Ocean Dynamics, 59*, 751–763. https://doi.org/10.1007/s10236-009-0231-4

[22] Mostamandi, S., Ukhov, A., Engelbrecht, J. P., Shevchenko, I., Osipov, S., & Stenchikov, G. (2023). Fine and coarse dust effects on radiative forcing, mass deposition, and solar devices over the Middle East. *Journal of Geophysical Research: Atmospheres*, *128*(22), e2023JD039479. https://doi.org/10.1029/2023JD039479

[23] Penlou, B., Roche, O., Manga, M., & van den Wildenberg, S. (2023). Experimental measurement of enhanced and hindered particle settling in turbulent gas–particle suspensions and geophysical implications. *Journal of Geophysical Research: Solid Earth, 128*, e2022JB025809. https://doi.org/10.1029/2022JB025809

[24] Petroff, A., & Zhang, L. (2010). Development and validation of a size-resolved particle dry deposition scheme for application in aerosol transport models. *Geoscientific Model Development, 3*(2), 753–769. https://doi.org/10.5194/gmd-3-753-2010

[25] R Core Team. (2023). *R: A language and environment for statistical computing* (Version 4.4.1).

https://doi.org/10.5194/egusphere-2026-261
Preprint. Discussion started: 26 May 2026

[Computer software]. R Foundation for Statistical Computing. https://www.R-project.org/

[26] Saylor, R. D., Baker, B. D., Lee, P., Tong, D., Pan, L., & Hicks, B. B. (2019). The particle dry deposition component of total deposition from air quality models: Right, wrong or uncertain? *Tellus B: Chemical and Physical Meteorology, 71*(1), 1–22. https://doi.org/10.1080/16000889.2018.1550324

[27] Shao, Y. (2008). Physics and modelling of wind erosion (2nd ed.). Springer. https://doi.org/10.1007/978-1-4020-8895-7

[28] Shao, Y., Raupach, M. R., & Findlater, P. A. (1993). Effect of saltation bombardment on the entrainment of dust by wind. *Journal of Geophysical Research, 98*, 12719–12726. https://doi.org/10.1029/93JD00396

[29] Slinn, W. G. N. (1982). Predictions for particle deposition to vegetative canopies. *Atmospheric Environment, 16*(7), 1785–1794. https://doi.org/10.1016/0004-6981(82)90271-2

[30] Sweeney, M. R., & Mason, J. A. (2013). Mechanisms of dust emission from Pleistocene loess deposits, Nebraska, USA. *Journal of Geophysical Research: Earth Surface, 118*, 1460–1471. https://doi.org/10.1002/jgrf.20101

[31] Tegen, I., & Fung, I. (1994). Modeling of mineral dust in the atmosphere: Sources, transport, and optical thickness. *Journal of Geophysical Research: Atmospheres*, 99(D11), 22897–22914. https://doi.org/10.1029/94JD01928

[32] Tian, L., & Ahmadi, G. (2007). Particle deposition in turbulent duct flows—comparisons of different model predictions. *Journal of Aerosol Science, 38*, 377–397. https://doi.org/10.1016/j.jaerosci.2006.12.003

[33] Waza, A., Schneiders, K., May, J., Rodríguez, S., Epple, B., & Kandler, K. (2019). Field comparison of dry deposition samplers for collection of atmospheric mineral dust: results from single-particle characterization. *Atmospheric Measurement Techniques, 12*, 6647–6665. https://doi.org/10.5194/amt-12-6647-2019

[34] Wesely, M. L. (1989). Parameterization of surface resistances to gaseous dry deposition in regional-scale numerical models. *Atmospheric Environment, 23*(6), 1293–1304. https://doi.org/10.1016/0004-6981(89)90153-4

[35] Wu, C., Lin, Z., & Liu, X. (2020). The global dust cycle and uncertainty in CMIP5 (Coupled Model Intercomparison Project phase 5) models. *Atmospheric Chemistry and Physics, 20*(17), 10401–10425. https://doi.org/10.5194/acp-20-10401-2020

[36] Wu, M., Liu, X., Yu, H., Wang, H., Shi, Y., Yang, K., Darmenov, A., Wu, C., Wang, Z., Luo, T., Feng, Y., & Ke, Z. (2020). Understanding processes that control dust spatial distributions with global climate models and satellite observations. *Atmospheric Chemistry and Physics, 20*(22), 13835–13855. https://doi.org/10.5194/acp-20-13835-2020

[37] Xin, Z., Liu, M., Zhang, J., and Wang, Z. (2024). A vertical expandable comprehensive recirculating wind tunnel for orbital platform (Chinese Patent No. CN117664498A). China National Intellectual Property Administration. Filed December 4, 2023; published March 8, 2024.

[38] Yu, M., Yu, X., Balachandar, S., & Manning, A. J. (2022). Floc Size Distributions of Cohesive Sediment in Homogeneous Isotropic Turbulence. *Frontiers in Earth Science, 10*, 815652. https://doi.org/10.3389/feart.2022.815652

[39] Zeng, Y., Wang, M., Zhao, C., Chen, S., Liu, Z., Huang, X., & Gao, Y. (2020). WRF-Chem v3.9 simulations of the East Asian dust storm in May 2017: Modeling sensitivities to dust

https://doi.org/10.5194/egusphere-2026-261
Preprint. Discussion started: 26 May 2026

emission and dry deposition schemes. *Geoscientific Model Development, 13*(4), 2125–2147. https://doi.org/10.5194/gmd-13-2125-2020

[40] Zhang, L., & He, Z. (2014). An empirical algorithm estimating dry deposition velocity of fine, coarse and giant particles. *Atmospheric Chemistry and Physics, 14*(7), 3729–3737, https://doi.org/10.5194/acp-14-3729-2014

[41] Zhang, J., & Shao, Y. (2014). A new parameterization of particle dry deposition over rough surfaces. *Atmospheric Chemistry and Physics, 14*(22), 12429–12440. https://doi.org/10.5194/acp-14-12429-2014

[42] Zhang, L., Brook, J. R., & Vet, R. (2003). A revised parameterization for gaseous dry deposition in air-quality models. *Atmospheric Chemistry and Physics, 3*(6), 2067–2082. https://doi.org/10.5194/acp-3-2067-2003

[43] Zhang, J., Shao, Y., & Huang, N. (2014). Measurements of dust deposition velocity in a wind-tunnel experiment. *Atmospheric Chemistry and Physics, 14,* 8869–8882. https://doi.org/10.5194/acp-14-8869-2014

[44] Zhao, K., Vowinckel, B., Hsu, T.-J., Bai, B., & Meiburg, E. (2023). Cohesive sediment: Intermediate shear produces maximum aggregate size. *Journal of Fluid Mechanics, 965*, A5. https://doi.org/10.1017/jfm.2023.380